Manuscript prepared for Atmos. Meas. Tech. Discuss.
with version 2014/09/16 7.15 Copernicus papers of the LaTeX class copernicus.cls.
Date: 24 June 2015

Measurement of atomic oxygen in the middle atmosphere using solid electrolyte sensors and catalytic probes

M. Eberhart[1], S. Löhle[1], A. Steinbeck[2], T. Binder[1], and S. Fasoulas[1]

[1]Institute of Space Systems, University of Stuttgart
[2]Airbus DS GmbH

Correspondence to: M. Eberhart
(eberhart@irs.uni-stuttgart.de)

Abstract

~~The~~ The middle- and upper atmospheric energy budget is largely dominated by reactions involving atomic oxygen (O). Modeling of these processes requires detailed knowledge about the distribution of this oxygen species. Understanding the mutual contributions of atomic oxygen and wave motions to the atmospheric heating is the main goal of the rocket ~~campaign WADIS~~ project WADIS (WAve propagation and DISipation in the middle atmosphere). It includes, amongst others, ~~two of~~ our instruments for the measurement of atomic oxygen that have both been developed with the aim of resolving density variations on small vertical scales along the trajectory. In this paper the instrument based on catalytic effects (PHLUX) is introduced briefly. The experiment employing solid electrolyte sensors (FIPEX) is presented in detail. These sensors were laboratory calibrated using a microwave plasma as a source for atomic oxygen in combination with mass spectrometer reference measurements. The spectrometer was in turn calibrated for O with a method based on methane. In order to get insight into the horizontal variability the rocket payload had instrument decks at both ends. Each housed several sensor heads measuring during both the up- and downleg of the trajectory. The WADIS ~~campaign~~ project comprises two rocket flights during different geophysical conditions. Results from WADIS-1 are presented which was successfully launched in June 2013 from Andøya Rocket Range, Norway. FIPEX data was sampled with 100 Hz and yield atomic oxygen density profiles with a vertical resolution better than ~~10~~9 m. This allows to study density variations on very small spatial scales. Numerical simulations of the flow field around the rocket were done at several points of the trajectory to assess the influence of aerodynamic effects on the measurement results. Density profiles peak at 3×10^{10} cm^{-3} at altitudes of 93.6 km and 96 km for up- and downleg respectively.

1 Introduction

Atomic oxygen (O) is a highly reactive species and a key element in a number of atmospheric processes. At high altitudes it is one of the major constituents of Earth's atmosphere and may cause erosion to exposed parts of spacecraft, especially on solar panels of satellites and the space station (Reddy, 1995). In the mesosphere and lower thermosphere (MLT) O is an important carrier of chemical energy and plays a significant role in the distribution of solar energy ~~(Hedin et al., 2009)~~(e.g. Hedin et al., 2009). Atomic oxygen is produced by photodissociation of O_2 and is then dispersed via various processes such as ~~global circulation and wave motions~~turbulent mixing. The chemical energy stored is released upon recombination and as the lifetime of the radicals is long in the upper regions the heating may occur at a large distance from the source, horizontally as well as vertically. On the other hand, atomic oxygen is also involved in the most important heat sink in the MLT, the radiation of CO_2 in the 15 µm-band, where the population of the relevant energy levels depends mainly on collisions with O ~~(Mlynczak, 1996)~~(e.g. Mlynczak, 1996). Determination of local atomic oxygen densities is therefore a necessity for detailed modeling of the atmospheric energy budget and understanding of the underlying physical processes. The demand for high spatial resolution requires in-situ measurement techniques and the altitudes of interest leave sounding rockets as the only appropriate instrument carriers.

In the past decades numerous experiments with a number of different measurement techniques have been flown on sounding rockets to retrieve profiles of atomic oxygen number densities. A method that is known to be very accurate is the use of cryogenic mass spectrometers where the shock front of the payload is 'frozen out', which minimizes the influence of the aerodynamics (e.g. Offermann et al., 1981). This accuracy comes at the cost of a very high system complexity. Several optical techniques have been used for in-situ measurements on rockets that probe emission, absorption or fluorescence of atomic oxygen or species that are linked to it by a known reaction chain. Measurement of the so-called airglow is a method with a rather low instrumental complexity which determines the intensity of natural emissions involving O reactions at various wavelengths (e.g. Offermann and Drescher, 1973).

This technique basically requires only photometers and appropriate filters. A key factor is the exact knowledge of the rate constants associated with the relevant reactions. A method with good sensitivity and selectivity uses resonant fluorescence of atomic oxygen in the VUV at 130 nm. The emission from a lamp is absorbed by O atoms and the resonantly scattered photons are collected by a photomultiplier (e.g. Thomas and Young, 1981). This instrument can be complemented with absorption measurements in the same wavelength (e.g. Gu Improvements on the accuracy could be made by using O_2 airglow measurements, carried out simultaneously, for calibration of the resonant fluorescence analysis (Hedin et al., 2009). A review of techniques for the determination of atomic oxygen densities aboard sounding rockets and satellites can be found in (Osborne et al., 2001).

In order to quantify both the contribution of dissipating gravity waves and of atomic oxygen to the atmospheric heating the ~~campaign~~ project WADIS has been set up (Gritzner and Rapp, 2011; Gritzner and Strelnikov, 2013). The project is led by the Leibniz-Institute of Atmospheric Physics (IAP) under a grant ~~by~~ from the German Aerospace Center (DLR). Several institutions provided rocket-borne experiments for the direct measurement of small scaled turbulences and various neutral and charged particles in combination with ground based observations using radar and lidar. The ~~campaign~~ project foresees two launches of sounding rockets in very different geophysical conditions, during winter- and summertime. The Institute of Space Systems (IRS) ~~operates two sensor systems both~~ contributes to this project with the development of two new sensor systems designed for the determination of atomic oxygen density profiles along the trajectory.

The first instrument called FIPEX (Flux-ϕ(Phi)-Probe-Experiment) is based on solid electrolyte sensors, a technique that has been successfully flown on a number of rocket missions. On TEXUS 34 (Technologische Experimente unter Schwerelosigkeit, 1996) a modified commercial lambda probe was employed to measure O_2 densities (Schrempp, 1996), followed by miniaturized sensors on the Russian capsules IRDT (Inflatable Reentry and Descent Technology, 2000) and IRDT-2 (Fasoulas et al., 2001). ~~These sensors~~ The sensors used in these campaigns, however, could not distinguish between molecular and atomic oxygen. A refined version with improved selectivity towards O was used in an experiment

on the International Space Station (2008) (Schmiel, 2009). WADIS is the first ~~campaign~~ project to employ this measurement principle for the determination of atomic oxygen densities aboard a sounding rocket. The sensors are very small in size, lightweight, with low power consumption and feature a high temporal and therefore spatial resolution.

The second sensor system named PHLUX (Pyrometric Heat Flux Experiment) measures temperature on two surfaces with different catalytic activities towards the recombination of atomic oxygen. The surface that promotes recombination receives a higher amount of chemical heat, leading to a temperature difference between the surfaces proportional to the incident atomic oxygen flux. Such catalytic probes have previously been used for atmospheric research on sounding rockets, albeit with a different design (Perov and Rakhmanov, 1977). We adopted a concept originally developed for ESA's re-entry capsule EXPERT (European eXPErimental Reentry Testbed) (Herdrich et al., 2005). A basic idea was to simultaneously operate two measurement systems based on different principles and yet very similar in overall size and position on the rocket.

The first sounding rocket of the WADIS ~~campaign~~ project was launched on June 27th, 2013 at Andøya rocket range in Andenes, Norway, at 23:52h UTC. The payload had two instrument decks, one fore and one aft. They were symmetrically equipped with FIPEX and PHLUX sensors, together with several other experiments: CONE (~~neutral and ion~~ COmbined measurement of Neutrals and Electrons, neutral and electron density, temperature, IAP (Rapp et al., 2001)), particle detector (IAP), positive ion probe (~~TU Graz)~~PIP) and Faraday antenna (electron density, TU Graz,~~photometers~~ (Friedrich et al., 2013)), a photometer measuring in the O_2 IR A-band at 1270 nm (atomic oxygen~~and noctilucent clouds, MISU), Faraday antenna (electron density, TU Graz), Langmuir probe~~, ozone) and one at 220 nm (noctilucent clouds (NLC), both from MISU Stockholm (e.g. Hedin et al., 2009, 2008 and a new fixed-bias Langmuir probe comprising surfaces with different work functions (electron density, Embry-Riddle). The payload had a constant, almost vertical orientation during the experimentation phase and the instrumentation of the rocket on both ends had the benefit of measurements during both up- and downleg of the trajectory which enables conclusions about the horizontal distribution of relevant parameters. An apogee of 115 km

was reached, 5 km short of the planned trajectory.
In this paper we present the applied measuring principles ~~and results from~~ of the two IRS sensor systems~~, with an emphasis on FIPEX data~~ . FIPEX data and the derived atomic oxygen density profiles will be discussed and compared to literature. Details about the PHLUX operation and its results will be published in a companion paper. ~~Atomic oxygen density profiles calculated from the flight data will be discussed and compared to literature.~~

2 Solid Electrolyte Sensor FIPEX

The so-called lambda-probe presents the most prominent example of a solid electrolyte oxygen sensor. It measures the oxygen concentration in automobile exhaust gases in order to regulate the motor's air-fuel ratio. This sensor type is based on a ceramic solid electrolyte, often yttria stabilized zirconia (YSZ). Due to the structure of its crystal lattice it is a conductor for oxygen anions, O^{2-}. If a suitable interface is provided gas phase oxygen may be built into this lattice. This is accomplished by applying an electronically conductive platinum electrode onto the electrolyte surface. Here a multi-step reaction occurs (e.g., Hertz, 2006, p. 24): Gaseous O_2 is transported to the electrodes by bulk diffusion; it is adsorbed dissociatively on the surface; the O atoms are then driven to electrochemically active sites by surface diffusion; here oxygen is reduced in a charge transfer step to O^{2-} by electrons delivered by the electrode; the ions are then built into vacant lattice sites of the electrolyte structure.
The active sites are essentially found on the so-called triple phase boundary where electrode, electrolyte and gas phase are in direct contact. As electrons are moved in the charge transfer reaction the electrical potential of the electrode changes until an equilibrium is reached. The steady state potential depends on the gas phase oxygen concentration. The

potential difference $\Delta\Phi$ between two electrodes facing unequal gas compositions is given by the Nernst equation (e.g., Oldham and Myland, 1994):

$$\Delta\Phi = \frac{RT}{nF} \ln \frac{c_1}{c_2} \tag{1}$$

R is the universal gas constant, T the absolute temperature, F is Faraday's constant and n the number of electrons involved in the reaction. The oxygen concentrations above two electrodes in different environments are given by c_1 and c_2. If one electrode is exposed to a defined reference atmosphere then the oxygen concentration on the other side can be determined by measuring the steady state value of $\Delta\Phi$. Such a sensor works according to the so-called potentiometric principle.

If an external voltage U_S is applied to the electrodes, superposing the Nernst potential, the system is forced out of equilibrium and oxygen ions are driven through the electrolyte from cathode to anode. This results in a net flow that is associated with an electrical current I_S measurable at the electrodes. So-called amperometric sensors make use of this principle and show a wide measurement range over several orders of magnitude of oxygen partial pressure. The net flow of oxygen ions persists if both electrodes are brought to the same environment. Without the requirement of a reference atmosphere these sensors can be designed with a compact planar layout. Commonly a third electrode is employed as a reference and the voltage U_S regulated such that the potential difference between cathode and reference is a constant value. The benefit of this is a linear dependence of the measured sensor current on oxygen pressure over a wide range.

An important factor for the sensor behavior is the electrode material. Besides being a good electronic conductor and being both thermally and chemically stable, it has to promote the dissociative adsorption of molecular oxygen. As stated before, platinum exhibits all these features (Schwandt and Weppner, 1997).

On the contrary, O_2 is not adsorbed on gold surfaces under high vacuum conditions, except in the case of impurities, e.g. silicon or calcium (Légaré et al., 1980; Pireaux et al., 1984), so that a sensor with gold electrodes responds to molecular oxygen to a much lesser

degree. However, gas phase atomic oxygen is adsorbed directly here and may readily be incorporated into the described reaction chain. This provides the possibility of designing sensors with a selective response to atomic oxygen by using gold cathodes.

All the reaction mechanisms on the electrodes and in the electrolyte are temperature dependent. In particular the ion conductivity of YSZ rises exponentially with temperature (Park and Blumenthal, 1989) and requires the sensor to be heated to about 500 °C. It should be noted that the sensor currents for both molecular and atomic types are proportional to the flux of particles onto their surfaces and therefore respond to the total pressure if exposed to a moving medium.

The design of the amperometric sensor elements used in this paper is shown in Fig. 1. A functional YSZ film was screen printed from a paste (Tosoh Corporation, Japan) onto an alumina substrate. Two electrodes with an interdigitated layout and a third reference electrode were screen printed on top of the YSZ layer. A resistance heater was applied to the back side of the alumina plate, again by means of screen printing. Platinum paste (Ferro 64120410, Germany) was used for both the electrodes and the heater; for the electrodes the paste was mixed with YSZ-powder (Tosoh Corporation, Japan) giving a porous layer with an increased triple phase boundary. Electrodes and heater were contacted with gap welded Pt-Ni leads.

In order to obtain sensors selectively sensitive to atomic oxygen the cathode was subsequently electroplated with gold. This was achieved by placing the sensors in an electrolyte solution (no. 530522, Dr. Ropertz GmbH, Germany), with a voltage of 3.0 V applied between cathode and a stainless steel counter electrode for 3 minutes at a current of 10 mA.

The electrical circuit used to control and read out the sensors is shown in Fig. 2. A ~~PI~~ controller stabilizes the potential between cathode and reference to 300 mV by adjusting the U_S voltage. The sensor signal is the current I_S measured between anode and cathode. The sensor element is kept at a constant temperature throughout the flight by regulating the resistance heater to a defined ohmic value. Two sensors are mounted together in a common aluminum housing, one with a golden and one with a platinum cathode, as ~~as~~ shown in

figure 3. The platinum sensor is sensitive to both molecular and atomic oxygen while the gold sensor selectively measures the O density. Two heat resistant ceramic elements hold the sensors in place and the leads are soldered to a LEMO connector.

This ensemble with two different sensors makes up a sensor head; to ensure redundancy three of these heads were mounted on each the fore and aft deck of the payload. The sensors were operated by custom designed electronics, one on each deck, connected to the heads by a thoroughly shielded cable. The sampling frequency of the sensor data was 100 Hz. Considering the rocket speed along the trajectory this results in a theoretical vertical resolution better than 9 m during the flight. The photograph given in Fig. 4 shows the final assembly of the instruments on the fore deck of the rocket, with both a FIPEX and PHLUX sensor head visible. Pairs of heads were distributed with a 120° spacing on an adapter ring. The FIPEX sensors were mounted parallel to the rocket axis so that their sensitive electrode surface is oriented perpendicular to the main component of the flight velocity. This orientation was chosen to minimize the influence of the rocket speed onto the measured oxygen flux.

3 Catalytic Probe PHLUX

Two oxygen atoms recombining on a surface release an energy of 5.2 eV (Hammer et al., 1999) leading to a temperature increase. The number of recombinations in a time interval depends on the flux of atoms onto the surface and on its catalytic activity towards this reaction, expressed by a recombination coefficient γ. The ~~surface temperature~~ heat flux can be related to the incident chemical heat and thus to the atomic oxygen density. To account for varying and unknown heat transfer coefficients from the surface to the surroundings a second inert probe is used. Its ~~temperature~~ heat flux variations reflect all other heat transfer mechanisms, like convection and radiation. In the PHLUX probe head two Pt100 temperature sensors (Heraeus type L220P, sensor area 2x2 mm^2) with different coatings, silicon dioxide (SiO_2) and platinum, have been placed close to each other. Platinum is a highly catalytic material, while SiO_2 is used as inert reference with γ close to zero. In order to

minimize heat losses to the structure the Pt100 elements are embedded in an aerogel pad (Airloy from Aerogel Technologies Inc., USA) with extremely low thermal conduction. To account for heat losses through the sensor lead wires the temperature of the connector pins is measured by a thermocouple. Figure 5 shows the complete sensor head with a PEEK housing. Similar to FIPEX two heads are mounted on each payload deck for the sake of redundancy.

According to the original schedule WADIS-1 was planned in winter time, in dim light or during night. Sunlight became an obstacle to the PHLUX measurements as plans had to be shifted to summer conditions. Solar radiative heat exceeds the chemical contributions on both the coated and the uncoated surface. As the absorption coefficients and their dependence on wavelength and temperature are not known exactly the concept was altered to rule out this source of error. One of the sensor heads was covered with a sapphire window, so that the surfaces beneath do not receive any chemical heat and the temperatures represent the pure solar contributions. These values can be subtracted from the results of the uncovered head, leaving the effect from atomic recombination, if convection is assumed to be identical on both heads . This step was omitted on the aft deck as no direct sunlight was expected here.

Custom electronics were used to read the temperature of the thermocouples and the resistance of the Pt100 elements. Four-wire measurement eliminated uncertainties due to different cable lengths. Sensor data was sampled with a frequency of 1000 Hz.

4 Calibration

As no first-principles model can be employed for the interpretation of the sensor readings a laboratory calibration is necessary. This applies especially to solid electrolyte sensors, for both molecular and atomic oxygen, but more generally also to the catalytic probes. Here parameters like the catalytic efficiencies, absorption and emission coefficients or other thermo-physical properties of the sensor design are only known with high uncertainties. In the following the calibration method for the FIPEX sensors is detailed. The PHLUX sen-

sors were calibrated for the incident heat flux density using the NISI (Non-Integer System Identification) method (Löhle et al., 2013, 2007).

A microwave generator (2.45 GHz, Sairem, France) is used to produce a low pressure oxygen plasma as a source for atomic oxygen, a technique widely employed in various technical and scientific applications and well studied in literature (Lebedev, 2010). The pure oxygen plasma is sustained within a cylindrical quartz tube at an oxygen pressure of 1.0 mbar and an incident microwave power of up to 300 W. The tube has a length of 30 cm with an outer diameter of 50 mm and a wall thickness of 2.5 mm and is mounted onto a vacuum chamber. The atomic oxygen generated in the discharge is expanded into the vacuum through a small orifice (⌀ 0.3 mm) along with undissociated molecular oxygen. This generates a fast beam with a distinct radial and axial distribution of the atomic oxygen density. In a first step the radial profile of the degree of dissociation in this beam is determined with a quadrupole mass spectrometer (QMS, Hiden HAL 3F with cross beam ion source). The QMS is mounted on a flexible bellow with its axis perpendicular to the beam. A mechanism allows variation of the radial position of the QMS thus recording the desired profile. The degree of dissociation is obtained as the ratio between the readings at mass numbers 16 (O) and 32 (O_2). To suppress dissociative products in the ion source, which corrupt the measurement, a low electron energy of 16 eV is used. As the QMS is operated with non standard parameters it in turn has to be calibrated. For this purpose we employ a method involving methane (CH_4) that shares mass number 16 with atomic oxygen (Agarwal et al., 2004). The energy scale of the ionizer is calibrated against the well know appearance potential of argon.

It should be stressed that the mass spectrometer only determines static number densities regardless of the velocity of the medium (Singh et al., 2000). However, the calibration of the sensors requires knowledge of the flux of O atoms in the beam. Therefore a second measurement is required to provide the total flux which can be combined with the degree of dissociation to form the profile of atomic oxygen total pressure needed for calibration. This measurement is made in the pure O_2 beam (plasma off) with a solid electrolyte sensor with platinum electrodes calibrated for O_2 under static conditions. As the beam profile is

radially symmetric this sensor is mounted on a linear/rotary manipulator (MDC BRLM-275) opposing the QMS, together with the atomic oxygen sensor to be calibrated. After the total flux profile has been determined the manipulator is turned about 180°, so that the second sensor is exposed to the beam and its response to the radially varying atomic flux (plasma on) can be recorded. This enables an almost simultaneous operation of the O sensor and the QMS reference system without the need of opening the vacuum chamber between measurements.

Calibration curves for atomic oxygen obtained by this procedure are given in Fig. 6 for the sensors used during WADIS-1. The different slopes of the curves are due to tolerances in the manufacturing of the sensors. Slight variations in the heater geometry and the position of the electrodes on the substrate, for example, lead to temperature differences that directly affect the sensor signal. Variations in the spacing between the electrodes furthermore result in a differing conductance across the electrolyte.

Calibration for molecular oxygen is done by testing the sensors in a vacuum chamber under stationary conditions. The partial pressure of O_2 is varied by a leak valve (Balzers UDV 235) and the sensor current measured against a pressure gauge (Pfeiffer FullRange PKR251). Results for one sensor (C24) with platinum cathodes are plotted exemplarily in Fig. 7. Values for the gold plated atomic oxygen sensor C15 are given additionally in this plot. All sensors with gold cathodes showed almost no sensitivity towards molecular oxygen in the relevant pressure range.

5 Aerodynamic considerations

It is important to consider that the measurements conducted on sounding rockets are intrusive because the rocket itself influences the flow field of the medium to be analyzed. The high velocities produce complex patterns of shock- and rarefaction waves with regions of very different temperatures and densities than in the undisturbed atmosphere. Due to their different masses and thermal velocities the abundance of the various species may

additionally be altered in the vicinity of the rocket walls (Bird, 1988). All such effects have to be taken into account when making conclusions on atmospheric properties from the measurement results. Exceptions are instruments with cryogenically cooled surfaces like the mass spectrometers flown on several missions (Offermann et al., 1981). Here incident particles are trapped on the cold walls and the shock is 'frozen out' as no reflections occur. This, however, requires intensive cooling with liquid helium to temperatures below 20 K which dramatically increases the system complexity. ~~Optical~~ Some methods may operate on a boom deployed from the rocket to probe a volume well outside of the shock front ~~(Hedin et al., 2009)~~(e.g. Hedin et al., 2009). Here aerodynamic simulations are required to reveal the position and extent of the disturbances to appropriately design the detection system.

In order to investigate the aerodynamic effects during the flight, we conducted simulations of the flow field at distinct points of the trajectory. These computations have to account for the transition of the flow regime from continuum to free molecular flow across the mesopause region, which cannot be treated by classical continuum mechanics. As indicated in Fig. 8 the WADIS payload had an almost vertical orientation throughout the whole experimentation phase so that three dimensional aerodynamics have to be considered due to the horizontal velocity component.

The Direct Simulation Monte Carlo method (DSMC) of the PICLas-code, developed in collaboration between IRS and the Institute of Aerodynamics and Gas Dynamics (IAG) (Munz, 2014), was employed to simulate the flow conditions at five points on the downleg part of the trajectory. For collisions a pairing scheme including the Natural-Sample-Size method with a nearest neighbor search and a standard (variable hard sphere, VHS) model was applied in which the energy dependent collision cross section is derived from viscosity data by $\mu \propto T^{\omega}$ ($\omega = 0.75$ used). The species Ar, O, N_2 and O_2 were considered in the calculation with a VHS reference temperature of 273 K. For the VHS reference diameters values of 4.17 Å (Ar), 3.1 Å (O), 4.17 Å (N_2) and 4.07 Å (O_2) were used.

The internal degrees of freedom of the molecules were taken into account while neglecting chemical reactions. Each particle in the simulation represented between 1.5x10^{11}

and 2x10^{13} real particles (macro particle factor, MPF). The computational domain includes an unstructured, hexahedral mesh with cell edge lengths between 3 mm and 50 mm and rectangular boundaries with minimal distances to the body ranging from 0.5 to 1.3 m. Symmetry of the rocket was exploited by simulating only one half of the domain. The sensor heads were included in the calculation with simplified block-like geometries with the approximate size of two adjoined heads. Apart from the actual triangular configuration, see sketch in Fig. 4, two of these blocks were positioned on adjacent sides of the rocket axis in order to cover both the maximal and minimal particle density cases during one revolution of the rocket. On the walls a diffusive reflection with full accommodation and a temperature of 300 K was assumed, whereas specular reflection was set for the plane of symmetry. All other boundaries were open with an inflow from a virtual buffer layer filled with particles of a Maxwell-Boltzmann distribution corresponding to the free stream condition. Steady state, i.e. start of averaging of macroscopic values, such as particle density, was assumed to be reached after 0.02 s. The gas composition at the different altitudes was taken from the standard MSIS-E-90 model ~~,~~ and temperatures from the CONE results where it is derived by integrating the measured neutral air density profile (Rapp et al., 2001). Sensitivity analyses were conducted in terms of varying boundary distances and MPFs. Computing time for the simulations ranged from 0.5 to 4 h on 96 cores of a CRAY XC40 for altitudes above 85 km and was 10 h on 192 cores for the 85 km case. Flow field results for 85 and 100 km altitude are given exemplarily in Fig. 9. Here the ratio of the local total number density (n) to the value of the undisturbed atmosphere (n^{∞}) is plotted. At 85 km a distinct shock is formed with pronounced ram and wake regions that are blurred towards higher altitudes. The values of n/n^{∞} on the upwind side at the sensor position are given in Fig. 10 as a function of altitude, with one line each representing the ram and wake sensors. The n/n^{∞} values were multiplied to the measurement results to correct for aerodynamic effects. Due to computational reasons only the total number densities could be considered for this ratio; in previously published simulations, however, the relative abundance of O was shown to vary only slightly (Hedin et al., 2009).

6 Results

In the following the results from the FIPEX measurements before and after aerodynamic correction are given. Number densities are calculated from the raw sensor signals by applying the linear relationships obtained from the individual calibration curves. The results are subsequently corrected for aerodynamic effects by dividing them by the appropriate ram- or wake-factors obtained from the numerical simulations. These factors were linearly interpolated for all altitudes from the curves given in Fig. 6.

Emphasis is laid on the atomic oxygen density profiles; values for molecular oxygen, obtained from the platinum cathode sensors, ~~and PHLUX results~~ are presented briefly. Interpretation of the PHLUX results still requires a thorough analysis that will be given in a companion paper.

6.1 FIPEX - atomic oxygen profiles

An overview of the raw signals obtained from all atomic oxygen sensors is given in Fig. 8. The values are plotted versus the duration of the flight, together with the altitude and significant events. Additionally the orientation of the rocket payload with instrument decks on both ends is shown. Due to their alignment the sensors were affected by the horizontal component of the flight velocity. As the rocket was spin stabilized this resulted in a signal modulated with a 2.9 Hz-component that was removed with a notch filter. One sensor on the lower deck showed unstable oscillations in the signal and was excluded from further analysis, so that in total results from ~~5~~ five O sensors could be used. After application of the respective calibration curves atomic oxygen partial pressures were obtained. Number densities were calculated by dividing by kT, were k is Boltzmann's constant and T the local absolute temperature measured with high spatial resolution by the CONE instrument. Temperature data was not available for altitudes above 110 km. The apogee of the trajectory was 115 km.

Fore sensors

Data obtained from the fore sensors before aerodynamic correction is given in Fig. 11. Corrected profiles are plotted in Fig. 14. In the initial phase, after nosecone separation at 53 km altitude, the sensors had to accommodate to the low density conditions of the free atmosphere~~and~~. Gases that have been adsorbed on the electrodes under atmospheric pressure before liftoff desorb from the surface. This process leaves the sensors in unstable condition and hence they show very different results in the beginning. They measured in the rocket ram during ascent and stayed in the wake during descent. The profiles are plotted from an altitude of 80 km upwards where they converge at 91 km to form a sharp rise in atomic oxygen number density. From that point onwards the curves follow each other qualitatively with a maximum ~~deviation of 2.5×10^{10} cm^{-3} at their peak~~ value at 93.6 km altitude. During downleg variations in the O density can still be resolved, with two profiles closely matching (C17 and B22) while the third one (C15) differs. The characteristics obtained by the first mentioned sensors are similar to the ascent results while their magnitude is reduced~~by a factor of about 3~~, with less details than during upleg.

Aft sensors

The motor was separated at an altitude of 60.9 km releasing the lower instrument deck. Profiles recorded by the aft sensors are plotted in Fig. 12, again without application of the aerodynamic correction factors. Corrected results are included in Fig. 14. While in the wake, during ascent, no density variations could be determined. For both sensors the downleg profile is dominated by a deep dip with a minimum between 104 and 106 km, followed by a gradual rise that peaks at 96 km altitude. Below that point a characteristic sharp gradient and small-scaled variations are observed, followed by a sharp gradient at an altitude of 87 km. The high frequency fluctuations in the lower part of the curves are probably leftovers from the rocket spin. The payload enters flat spin at around 68 km which terminates the measurements. Below 85 km the results suffer from increasing noise ~~that may be~~ due to a beginning instability in the flight state~~or due to increasing thermal load at higher density~~

~~levels~~.

6.2 FIPEX - molecular oxygen

Results for the molecular oxygen number density recorded by sensor C24 (fore deck) during the upleg and downleg after aerodynamic correction with the ram- and wake-factors, respectively, are plotted exemplarily in Fig. 13. Here the calibration curve given in Fig. 7 was applied to the raw signal after filtering out the spin modulations. This practice neglects the fact that the platinum electrodes also respond to atomic oxygen, although with a different characteristic than to O_2 due to differing adsorption kinetics. ~~On the one hand the binding energy of the molecule has to be supplied for the dissociative adsorption to take place and on the other hand the~~ The probability of finding suitable neighboring adsorption sites ~~for both atoms~~ on the surface for both atoms is lower than in the case of a single incident O atom. The complete calibration of a platinum sensor for mixtures of O_2 and O is therefore more complex than in the case of gold electrodes that do not respond to molecular oxygen. For this reason the results cannot be understood as pure O_2-profiles but represent in some way the sum of atomic and molecular oxygen number densities. An approximate equation describing the total signal of a sensor with platinum electrodes as a sum of the contributions from O and O_2 is given in (Förstner, 2003). However, in order to separate the measured currents into their components a detailed knowledge of electrode properties such as their surface area, total number of adsorption sites or adsorption probabilities of the species is required.

~~The FIPEX profile obtained by the fore sensor C24 during the upleg is qualitatively very similar to the MSIS curve while being lower in absolute values. The altitude of 93 is marked by the sharp rise in atomic oxygen density that begins to influence the results.~~ The fact that up- and downleg-profiles are very close in their absolute values is an indication for a realistic numerical modeling of the aerodynamics, resulting in appropriate correction factors for both ram- and wake-sensors.

7 Discussion

The FIPEX density profiles after application of the aerodynamic corrections are given in Fig. 14. Additionally, ~~results from the PHLUX measurements are plotted and~~ data is compared to the standard MSIS-E-90 model. Though having been measured in different geophysical conditions profiles obtained during the NLTE-2 campaign, launched at Esrange rocket range, northern Sweden, on March 6th, 1998, are additionally included for comparison (Hedin et al., 2009).

A fair agreement is observed for the altitude of maximum O number densities between the FIPEX results and the MSIS and NLTE-2 data. FIPEX profiles peak at 93.6 km and 96 km for the up- and downleg, respectively. The MSIS-E-90 curve shows a peak value at 93.5 km and the NLTE-2 measurements recorded a maximum at 97.5 km altitude. The NLTE-2 results have a much higher spatial resolution (smoothed to 250 m on the vertical axis) than the MSIS profile and feature several distinct local extrema. The absolute peak values for n_O from MSIS and NLTE-2 are higher than the FIPEX results by factors of 5 and 14, respectively.

Both fore and aft sensors recorded variations in atomic oxygen number density on a scale that is beyond the spatial resolution of the MSIS-E-90 and NLTE-2 profiles. The results show local extrema that can mostly be found in the curves recorded from the others sensors on the same instrument deck while they differ slightly in altitude and absolute value between upleg-fore and downleg-aft measurements. These differences ~~might be interpreted as~~ are intended to be linked to horizontal variations in O density as the trajectory spans over a distance of about 30 km at 80 km altitude. The broad minimum observed in the downleg-aft profiles at around 105 km altitude, is, however, most likely not due to actual large variations in the atomic oxygen concentration; the fore sensor data does not show this feature. One attempt for explaining this situation could be made by assuming the onset of outgassing on the rocket rear side beyond apogee. The surfaces would heat up due to an evolving bow shock releasing adsorbed particles, e.g. exhaust gases, that consume atomic oxygen in chemical reactions. However, the increase in surface temperature measured by the

PHLUX sensors between apogee and 105 km was only about 0.5 K, so that outgassing does not seem to cause an atomic oxygen depletion. We favor an interpretation based on the electrode kinetics. As laid out before, the reference voltage of the sensor is regulated to a constant value by appropriately adjusting U_S, the voltage between anode and cathode. With increasing oxygen concentration U_S has to be raised which leads to a linear characteristic of the sensor current over a wide pressure range. Under steady state conditions a given oxygen density can be attributed to a certain ratio of U_S and I_S values. During downleg a rise in this ratio along with a decline in the absolute U_S value can be found in the aft sensor data, see Fig. 15, exactly at the altitude were the dip in O density was observed. Although the gold coated cathode is not sensitive towards molecular oxygen the platinum reference electrode still dissociatively adsorbs O_2. Its reduction to O^{2-} consumes electrons which increases the potential difference between reference and cathode. Subsequently U_S is lowered by the controller to maintain a constant reference voltage, leading to a decrease in I_S. This mechanism is believed to cause the dip in the signal after the sensors left the rocket wake with a very low O_2 density beyond apogee.

At very low ambient pressures the coverage of the electrode surfaces with adsorbed oxygen is also low. For two reasons the coverage on the cathode is further reduced compared to the other electrodes: Firstly, gold prevents adsorption of molecular oxygen with only very low O concentrations in the rocket wake and, secondly, adsorbed O is pumped away by the applied voltage U_S. Surface diffusion to the triple phase boundary is slowed down at these low coverages so that a steady state is reached only after long periods (Förstner, 2003, p. 106). The described slow kinetics may also explain the delayed onset of the effect some seconds beyond apogee.

Further investigations into the transient reaction of the sensors at very low pressures have to be carried out; this will also help to improve the interpretation of high frequency variations of the results in that regime.

~~For upcoming missions the use of sensors with all-golden electrodes should be considered to eliminate the issues generated by different reactions on different electrode materials. A further consequence of~~ Generally speaking the results recorded in the ram, i.e. the

fore-upleg and aft-downleg profiles, appear to reflect the actual variations better than their counterparts in the wake. In the ram the measurements are also influenced by aerodynamic effects, but the response to density variations is obviously more direct, showing fluctuations on a smaller scale with a better signal-to-noise ratio.

A comparison of the ~~findings described here might be an operation of sensors with a fixed U_S, i. e. without regulating the reference voltage. This helps to maintain the electrical conditions used during laboratory calibrations at~~ fore- and aft-results during downleg is given in Fig. 16, together with the MSIS-E-90 profile which has been scaled by a factor of 0.5. The curves have been corrected by the aerodynamic factors for ram and wake, respectively. Though different in magnitude the obtained profiles agree widely on a qualitative basis. Small scaled features are represented in all curves, e.g. the short dip at 89 km altitude or the steps at 87 km and 93 km. The fact that these results are simultaneously recorded at opposite ends of the rocket with different sensors on individual electronics increases confidence that actual atmospheric O density variations were measured. The deviation between the profiles of one side, especially among the fore sensors, is most likely caused by the U_S voltage control. The course of U_S during downleg is given in the inset of Fig. 16. These curves reflect the long scaled differences obtained in the number densities from the single sensors. A U_S voltage control in combination with electrodes from different materials (golden cathode, platinum anode and reference) apparently accentuates deviations between the sensor properties that are due to the ~~expense of increased nonlinearity of the calibration curve~~mentioned manufacturing tolerances. Variations in the surface- and triple phase boundary-ratio between the golden cathode and the other electrodes can thus lead to a different controlling behavior in a mixed O_2/O atmosphere. While the voltage control is a versatile instrument to maintain stable conditions on the cathode for sensors with electrodes made from identical materials, e.g. all-platinum electrodes for sensing pure O_2, it seems to corrupt the measurements in the present case.

Uncertainties, sources of error and recommendations

Several possible sources of errors and uncertainties in the calibration procedure as well as during the flight experiment can be identified that are addressed in the following.

During calibration the sensors are exposed to atomic oxygen produced in a microwave discharge. The atoms might be accompanied by other oxygen species influencing the sensor signal, with a focus on ozone (O_3) and electronically excited molecular oxygen O_2^*, especially in its long-lived $^1\Delta_g$-state (so-called singlet oxygen). In both cases it is important to investigate whether the species can contribute to the measured sensor current and if they are actually present in the experiment. In order to answer the first question the initial step of the electrode reactions, the adsorption on the gold surface, is regarded. It can be found in the literature that ozone does adsorb on gold and hence will be part of the reaction chain forming the sensor signal (Saliba et al., 1998; Kim et al., 2006). For singlet oxygen relevant literature is very rare; there are practically no publications that examine if O_2^* is, in contrast to ground state O_2, adsorbed on gold surfaces or not. A hint is given in the work by Gottfried et al. where weakly bound physisorbed oxygen is adsorbed by electron bombardement (Gottfried et al., 2002). They discuss that a threshold electron energy of 3.5 eV is required for this process. The excitation energy of O_2 $^1\Delta_g$ is listed, on the other hand, as 0.98 eV (Herzberg, 1950). On that basis it could be speculated that this species does not possess the necessary activation energy for adsorption, albeit the two underlying processes are different.

The abundance of ozone during calibration was checked by recording the QMS signal at mass number 48. Only minute trace amounts of ozone could be found, although the cross section for electron impact ionization of O_3 in the QMS ion source is higher than for O_2 (McConkey et al., 2008). Ozone is not produced directly in the discharge but in its afterglow via recombination of atomic oxygen (Normand et al., 1995). In the present setup the afterglow is too short to release significant amounts of ozone into the vacuum chamber. The detection of O_2^* is, however, not straightforward. We employed a method that seeks to identify singlet oxygen in the threshold ionization curves obtained by scanning the electron energy in the QMS ionizer (Herron and Schiff, 1958; Pulpytel et al., 2005). Excited molecules are already ionized at lower electron energies and so leave traces in the curves at energies

lower than the appearance potential of the ground state molecule. In order to avoid production of excited species from other sources all ionization gauges were turned off during the experiments. Curves with scanning electron energies were recorded for both plasma-on and -off conditions with the energy scale calibrated against the appearance potential of argon. The curves were normalized to their value at 40 eV and averaged over about 100 single scans. In both cases the results were identical and did not confirm the presence of O_2^*. Though it is most likely produced in the microwave discharge it probably suffers from deactivation at the silica walls during the passage through the orifice. With a diameter of 0.3 mm and a length of 2.5 mm it forms a narrow tunnel where multiple wall collisions occur before the molecules exit into the high vacuum. It should be noted~~that the sensor currents measured~~, however, that in contrast to the calibration conditions both ozone and O_2 ($^1\Delta_g$) have been measured in the atmosphere aboard sounding rockets, with peak densities in 90 km altitude of about $1x10^8$ cm^{-3} and $3x10^9$ cm^{-3} for ozone and O_2 ($^1\Delta_g$), respectively (Gumbel et al., 1998). These species could then contribute to the uncertainties in the atomic oxygen measurements. It is therefore important to further investigate their effect on the sensor signals.

It was revealed in recent experiments that the electron energy in the QMS ionizer is influenced by the microwave plasma and thus can deviate from its nominal value. More precisely it is shifted to lower energies when the discharge is turned on. This shift, however, affects both the QMS results for O_2 and for atomic oxygen. Their ratio is the relevant quantity for the calibration and with an observed energy deviation of 1.5 eV the measured atomic oxygen density would be low by 8%, based on the literature values for electron impact ionization (Laher and Gilmore, 1990; McConkey et al., 2008).

Calibration of the QMS is done by recording its readings at a series of partial pressures of O_2 and CH_4, respectively, compared to the output from a cold cathode gauge (Pfeiffer PKR 251) with an accuracy of $\pm$ 30%. The correction factor for CH_4 of the cold cathode gauge was found with the aid of a precise, gas-type independent capacitance manometer (MKS Baratron 690A, accuracy $\pm$ 0.12%) in the pressure range above 10^{-6} mbar. Linearity was assumed below that point.

A shortcoming of the calibration method in its present form is its inability to cover the complete range of atomic oxygen number densities encountered during the flight experiment. The sensor currents measured along the trajectory, see Fig. 8, exceed the signals given in the calibration curves, see Fig. 6. Their linear characteristics had to be extrapolated by a factor of approximately 3.5. ~~At~~ However, at a certain pressure the respective curves will become nonlinear. This is a gradual transition and depends on parameters such as material, surface, geometry and temperature of the electrodes and the electrolyte. If the flux of oxygen delivered by the electrodes via surface diffusion exceeds the rate at which it can be transported to the anode the current-pressure curve flattens. For the molecular oxygen sensors this is observed at currents beyond 10 µA, see Fig. 7. The O sensors differ in a thin layer of gold on the cathode which will only very slightly alter its total surface area or the length of the three phase boundary, so that a linear behavior is assumed here up until the levels observed in the flight. Neglecting an actual nonlinearity in the characteristics, however, would lead to an underestimation of the number densities~~, which might contribute to the differences in absolute values between measured profiles and the MSIS-standard or the NLTE-2 results~~.

~~Generally speaking the results recorded in the ram, i. e. the fore-upleg~~ A major uncertainty during the flight is due to the sensor voltage U_S. As laid out before, the golden cathode is widely inert towards molecular oxygen, but the other electrodes are not. This means that the controller may adjust a U_S different to the value during calibration if the O/O_2 ratios in both cases differ. Apart from the 'dip' in the profiles discussed earlier this also affects the total signal level. In fact, sensor voltages of less than half of the value applied during calibration were observed. There is, however, no direct linear relation between U_S and ~~aft-downleg profiles, appear to reflect the actual variations better than their counterparts in the wake. In the ram the measurements are also influenced by aerodynamic effects, but the response to density variations isobviously more direct, showing fluctuations on a smaller scale with a better signal-to-noise ratio. Additionally, here not the full length of the rocket has to be considered in numerical calculations when trying to simulate the flow conditions along the trajectory. Though different in magnitude it is nevertheless informative to compare~~

the fore- and aft-results during downleg as I_S; this depends vastly on pressure and oxygen coverage of the electrodes. It is therefore hardly possible to recover the true signal based on the knowledge of the true U_S-value. Nevertheless we estimate that the recorded signals could be low by 50% due to this effect.

A clue about the total accuracy of the present methods can be obtained by comparing the absolute values of the results given in Fig. 16. Here the values of the fore-sensor B22 have been scaled by a factor of 3. Below 98If the uncertainties from the calibration are taken into account then the atomic oxygen number densities at the 96 kmaltitude most of the small scaled features of the aft deck sensor CO2 can also be found in the B22 curve at the same altitude. The fact that these results are simultaneously recorded at opposite ends of the rocket with different sensors on individual electronics increases confidence that actual atmospheric -peak differ by a maximum factor of about 6.4 between the fore- and aft sensors during downleg. This includes the aerodynamic correction based on the numerical simulations. The results from the fore sensors here suffer from a lower signal-to-noise ratio and the rise in O density variations are represented. density below 85 km most likely does not reflect the actual conditions. If the ram- and wake factors are assumed to be correct, based on the consistent results of the O_2 sensor in Fig. 13, then the high signals in the ram obviously underestimate the true number density. As discussed before this would be the case for an actual non-linearity in the calibration curves. A further indication of such non-linear characteristics can be found when regarding the magnitude of the rise in O concentration between 80 km altitude and the peak values at about 95 km. The results at the lower end of the profiles coincide well with the values measured in the NLTE-campaign. A more appropriate comparison is the NLC-93 campaign, launched in geophysical conditions similar to the WADIS-1 flight (July-August, night-time but sunlight at a high latitude), which also showes according results for the low altitudes (Gumbel et al., 1998). The values at 80 km are given as 3.2×10^9 cm^{-3} (NLTE), 2.4×10^9 cm^{-3} (NLC-93) and the present data reads 3.4×10^9 cm^{-3} for the aft sensors during downleg. However, the rise in O density to the peak value is clearly smaller than in the mentioned references. A non-linearity in the sensor characteristics could again be responsible for this underestimation of the high densities.

The maximum difference in the results between the aft sensors alone is below 15%, which leads to the conclusion that accurate measurements with the described technique are possible if the discussed sources of error can be ruled out in future experiments.
For upcoming missions the use of sensors with all-golden electrodes should be considered to eliminate the issues generated by different reactions on different electrode materials. A further consequence of the findings described here might be an operation of sensors with a fixed U_S, i.e. without regulating the reference voltage. This helps to maintain the electrical conditions used during laboratory calibrations at the expense of increased non-linearity of the calibration curve.
A way to shorten the initial unstable accommodation phase, observed especially for the front sensors, could be to cover the sensor heads with an evacuated housing that is separated together with the nosecone or the motor, respectively. Such a procedure is already realized for the CONE instrument. The housing should be pumped down to the pressure expected at the altitude of separation in order to minimize the desorption of gases from the electrodes.

8 Conclusions

The FIPEX instrument, based on solid electrolyte sensors, was for the first time used to measure atomic oxygen number densities on a sounding rocket and has successfully recorded profiles along the trajectory of WADIS-1. On a qualitative basis the results compare well with the MSIS standard atmosphere and the profiles obtained in the NLTE-2 campaign~~, but exceeding their resolution and recording density variations on small spatial scales. By symmetrical instrumentation on fore and aft deck it was possible to measure profiles both during the up- and downleg, which enables the detection of density variations on a horizontal scale~~. Measurements with the PHLUX instrument were complicated by solar radiation and require further analysis. The absolute values ~~measured with FIPEX~~ derived from FIPEX data in the ram are by factors of around 5 ~~to 14~~ and 13 lower than the mentioned references. The wake results on the contrary peak at values reduced by factors of 1.8 and 4.6, respectively. This might be due to nonlinearities in the sensor characteristics at

higher atomic oxygen densities that could not be covered in the laboratory calibration. Here further investigations are needed. Controlling of the sensor voltage in combination with electrodes made from different materials was identified as a key source for uncertainties during the flight. For upcoming missions sensors with all golden electrodes should be considered which may eliminate disturbances through different reactions of oxygen on platinum /and gold electrodes.Profiles for

The measurements stand out due to a unprecedented high spatial resolution, showing O number densities could also be calculated from PHLUX data, despite difficulties caused by solar radiation. If shifted upwards by 16 these profiles are qualitatively comparable to FIPEX results. density variations on very small vertical scales. The sensors are small and lightweight and thus enable a symmetrical instrumentation on fore and aft deck in order to measure profiles both during the up- and downleg in the same ram or wake conditions. This facilitates the detection of O density variations on a horizontal scale.

Acknowledgements. This work has been funded by the German Aerospace Center. We thank J. Hedin from MISU, Stockholm, for providing the NLTE data and B. Strelnikov, IAP Kühlungsborn, for the CONE temperature results. We appreciate the work from M. Hartling, IRS electronics lab, who designed the sensor electronics. The efforts of DLR MORABA and the support during the launch campaign are highly recognized. The platinum electrode sensors have been produced by ESCUBE GmbH in collaboration with our institute.

9 AUTHOR'S RESPONSE

We would like to thank the referees for their efforts in critically commenting our manuscript. The questions and suggestions haven been picked up and considered thoroughly for the revised version of the paper. All major points noted by the referees and some of the minor points requiring a detailed answer are addressed below.

9.1 Reply to Anonymous Referee #1

1. Yes, we have considered the possible effects of both $O_2(^1\Delta)$ and ozone on the sensor signal. A series of experimental investigations has been carried out to determine the abundance of these species. For ozone the measurements could be done with classical mass spectronomy (quadrupole mass spectrometer, QMS) on mass number 48, for $O_2(^1\Delta)$ the procedure is more complicated and requires to scan the electron energy in the QMS ionizer to reveal the presence of excited molecules. For both species it could be confirmed that they are not present in the setup used for sensor calibration. Ozone is not produced directly in the discharge but only in its afterglow from recombining oxygen atoms. In our case this afterglow is very short as the plasma products are directly expanded into high vacuum. The transition from the discharge tube into the calibration chamber requires the molecules to pass through a relatively long (2.5 mm) and narrow (⌀ 0.3 mm) orifice, where multiple wall collisions take place. This is likely to deactivate the $O_2(^1\Delta)$.
   Though this influence on the sensor signal could be ruled out we agree that it is of interest to the reader to discuss this possibility. We have included a section about uncertainties and sources of error in the discussion part of the paper where we detail the described findings and also discuss possible influences on the sensor in cases where ozone and $O_2(^1\Delta)$ are present. On the other hand it is important to consider that both mentioned species actually exist in the MLT region, albeit with lower concentrations than expected in a microwave discharge. Atmospheric measurements have been made e.g. in the NLC-93 campaign (Gumbel et al., JGR, Vol. 103, No. A10, pp. 23,399-23,1998). We have inserted this fact in the section about possible sources of error.

2. In order to investigate the possible influence of a non-linearity in the sensor characteristics not covered by the calibration we have altered Figure 16, the comparison between fore/wake- and aft/ram-results during downleg. Instead of scaling the wake-values by an arbitrary factor of 3.0 we have applied the actual aerodynamic correction factors derived by the numerical simulation. The O density profiles then obtained by the wake sensors are about 6 times higher than the ram-results. This implies that the densities

derived from high sensor signals are underestimated compared to those that result from the low signals in the wake. This could be explained by a non-linearity towards the upper signal levels.
As a further possible source of error to the absolute values not described in the initial manuscript we have identified the sensor voltage control in conjunction with electrodes made from different materials. This can (and did) lead to voltages that differ from those applied during calibration. Although a quantification of the effect on the sensor is difficult we estimate a possible reduction of the signals of 50% due to this effect.
We have detailed the discussion about these points in the section dealing with uncertainties and error sources.
Below 80 km the signals suffer from a very high noise level on the downleg (beginning instability in the flight state, flatspin) and from unstable initial conditions after nosecone ejection on upleg. For the sake of clarity these data have not been plotted in the diagrams. In the manuscript we have detailed the description of this unstable beginning phase that is marked by divergent profiles obtained from the single sensors. It continues on the upleg up to about 90 km. We have added the recommendation to house the sensors in an evacuated hood that is removed together with the nosecone/motor. This would minimize the desorption processes that are the cause of the observed instability and could yield reliable data right after the sensors are exposed to the atmosphere.

3. In fact, the results for the O concentration below 82 km coincide well with the values measured in the NLTE-campaign. A more appropriate comparison is the NLC-93 campaign, launched in geophysical conditions similar to the WADIS-1 flight (July-August, night-time but sunlight du to high latitude) (Gumbel et al., JGR, Vol. 103, No. A10, pp. 23,399-23,1998), which showed according results for this altitude. The values at 80 km are given as 3.2×10^9 cm^{-3} (NLTE), 2.4×10^9 cm^{-3} (NLC-93) and the present data shows 3.4×10^9 cm^{-3} for the aft sensors during downleg. However, the rise in O density to the peak value measured at around 95 km is smaller than in the mentioned references, and we suspect again a non-linearity in the sensors characteristics to be responsible

for this underestimation of the high densities.
This argument is now included in the discussion part of the manuscript.

4. This "bite-out" in the profile and the divergence of the curves from the single sensors occur during the beginning of the upleg and are most likely due to the instability of this initial phase, as discussed in the reply to point 3. The aft sensors track well because the results stem from the downleg measurements, where the sensors are in stable condition.

5. The PHLUX profile was shifted by 16 km in an attempt to find coincidence with the FIPEX curves. The reason for this shift is yet unclear. Analysis of the PHLUX data was complicated by the (unplanned) sunlight during the flight and has to be deepened to be able to properly interpret these result. Following the recommendation of the second referee we left the presentation of the PHLUX data for a future companion paper focusing on this instrument and restricted ourselves to the explanation of the measurement principles.

9.2 Reply to Anonymous Referee #2

1. We agree that even though (or *because*) this paper describes the very first application of solid electrolyte sensors for the measurement of atomic oxygen on sounding rockets it is desirable to learn more about the accuracy and possible sources of errors associated with this technique. For the calibration the main uncertainty is due to pressure measurements with a cold cathode gauge (accuracy $\pm$ 30%); additional uncertainties arise from a possible shift of the electron energy in the ionizer of the mass spectrometer that would lead to an underestimation of the O densities by 8%. We have introduced appropriate error bars in the calibration curves and show the related range of uncertainty in the processed density profiles.
The fact that the upper end of the sensor signals that occurred along the trajectory could not be covered by the lab calibration leaves an uncertainty due to a possible non-linearity towards higher signal levels.

During the flight we identified the control of the sensor voltage U_S, in conjunction with electrodes made from different materials, as a key source of error. The cathode is gold plated while the other electrodes have a platinum surface, and this leads, through the back door, to a dependency of the sensor reactions on the present molecular oxygen. This could affect both the qualitative and quantitative results of the measurements. We estimate that the absolute values could be low by 50% due to differences in sensor voltage between calibration and flight.
As mentioned in the reply to referee #1 we have inserted a section in the discussion dealing in detail with uncertainties and sources of error. We conclude with the recommendatio to use sensors with all-golden electrodes in further campaigns to enhance the reliability of the method.

2. The differences in the results from the individual sensors of one side are especially apparent on the fore deck, where the single profiles deviate also qualitatively. Again we identified the voltage control as a source of this behavior. We included a sub-plot additionally showing the course of U_S on the downleg illustrating this situation.
During upleg, on the other hand, a second effect dominates: Gases that have been adsorbed on the electrodes under atmospheric conditions desorb after the pressure drop following nosecone separation. Together with the voltage control this leaves the sensors in an initial unstable phase with results differing both qualitatively and in absolute numbers. These explanations are now all included in the discussion of the manuscript. As already stated in the reply to point 1 from referee #1 we recommend to house the sensors in an evacuated hood that is removed together with the nosecone, which would shorten this initial desorption phase.
The maximum difference in the results between the aft sensors alone, which also track well qualitatively, is below 15%, which leads to the conclusion that accurate measurements with the described technique are possible if the discussed sources of error can be ruled out in future experiments.

3. As given in the reply to the first referee we agree that the PHLUX data should be discussed separately in a future publication when interpretation of the results on the basis of a detailed analysis is possible. We would however like to keep the technical description of the instrument and of the measurement principle in this paper in order to give a complete overview of our contributions to the project.

4. We understand that it is desirable to interpret the results in terms of atmospheric-physical processes. This is, however, beyond the expertise of our institute. The interpretation of the profiles of atomic oxygen densities is greatly facilitated if the measurements from the other instruments, e.g. the electron densities, and the accompanying radar/lidar data are taken into account. We have detailed the description of all the instruments on the payload and have inserted appropriate references. The comparison to the O results deduced from the O_2 dayglow photometer measurements would also be of great interest in that respect. A future publication, probably led by the Institute of Atmospheric Physics, may link the findings on the various quantities.
   As the effect of mesospheric ice particles onto the very thin coatings of the PHLUX sensors was unclear conditions with few noctilucent clouds (NLCs) were favored for the launch. The actual distribution of ice layers can probably be retrieved from the NLC photometers measuring at 220 nm.

5. The background about techniques used in past campaigns for measuring atomic oxygen aboard sounding rockets has been extended in the introduction of the manuscript.

– Page 3250, line 22: The question if impurities on the gold surfaces of the electrodes are an issue for the measurements is answered by testing the O sensors additionally in pure O_2 atmosphere. We have added a “calibration curve” for the sensor C15 (gold plated cathode) in the manuscript that confirms its inertness towards molecular oxygen.

– Page 3255, line 10: see above.

- Page 3257, line 14-15: Yes, the results were divided by this factor. Factors at intermediate altitudes were interpolated linearly between those obtained directly from the simulations. This is now explained in the text.
- Page 3259, line 16: Downleg data is now included in this figure.
- Section 6.2: An approximate equation describing the total signal of a sensor with platinum electrodes as a sum of the contributions from O and O_2 is given in the dissertation of R. Foerstner (listed in the literature). However, in order to separate the measured currents into their components a detailed knowledge of electrode properties such as their surface area, total number of adsorption sites or adsorption probabilities of the species is required. We have added this argument in the explanations.
- Figure 6: It would be desirable to have sensor with all identical calibration curves. The different slopes, however, are due to tolerances in the production via screen printing. This means deviations in the heater and electrode geometries and their relative position, which in turn causes small variations in the temperature of the electrolyte and the electrodes. Slightly different spacings between the electrodes produces differences in the conductance across the electrolyte. Oxygen densities were calculated by applying the linear relations from the calibration curves to the measured sensor signals.We have detailed that in the explanation of the calibration results.
- Figure 14: Although the plot easily gets busy we would like to show the direct comparison between the results from fore deck-upleg and aft deck-downleg, as they are all obtained under ram conditions and this also include the horizontal variability of the profiles. However, we have removed the PHLUX results which helps to tidy up the figure.

References

Agarwal, S., Quax, G., van de Sanden, M. C. M., Maroudas, D., and Aydil, E.: Measurement of absolute radical densities in a plasma using modulated-beam line-of-sight threshold ionization mass spectrometry, J. Vac. Sci. Technol. A, 22, 71–81, doi:10.1116/1.1627767, 2004.

Bird, G. A.: Aerodynamic Effects on Atmospheric Composition Measurements from Rocket Vehicles in the Thermosphere, Planet. Space Sci., 36, 921–926, doi:10.1016/0032-0633(88)90099-2, 1988.

Fasoulas, S., Förstner, R., and Stöckle, T.: Flight Test of Solid Oxide Micro-Sensors on a Russian Reentry Probe, 2001-4724, AIAA, Space 2001 Conference and Exposition, 2001.

Förstner, R.: Entwicklung keramischer Festelektrolytsensoren zur Messung des Restsauerstoffgehalts im Weltraum, Ph.D. thesis, Institut für Raumfahrtsysteme, Universität Stuttgart, 2003.

Friedrich, M., Torkar, K. M., Hoppe, U. P., Bekkeng, T. A., Barjatya, A., and Rapp, M.: Multi-instrument comparisons of D-region plasma measurements, Ann. Geophys., 31, 135–144, doi:10.5194/angeo-31-135-2013, 2013.

Gottfried, J., Schmidt, K. J., Schroeder, S. L. M., and Christmann, K.: Spontaneous and electron-induced adsorption of oxygen on Au(110)-(1x2), Surface Science, 511, 65–82, doi:10.1016/S0039-6028(02)01555-8, 2002.

Gritzner, C. and Rapp, M.: ECOMA and WADIS, DLR Countdown, 15, 2011.

Gritzner, C. and Strelnikov, B.: Rough Seas in the Middle Atmosphere, DLR Countdown, 23, 2013.

Gumbel, J., Murtagh, D. P., Espy, P. J., Witt, G., and Schmidlin, F. J.: Odd oxygen measurements during the Noctilucent Cloud 93 rocket campaign, Journal of Geophysical Research: Space Physics, 103, 23 399–23 414, doi:10.1029/98JA02155, 1998.

Hammer, B., Hansen, L. B., and Norskov, J. K.: Improved adsorption energetics within density-functional theory using revised Perdew-Burke-Ernzerhof functionals, Phys. Rev. B, 59, 7413–7421, doi:10.1103/PhysRevB.59.7413, 1999.

Hedin, J., Gumbel, J., Khaplanov, M., Witt, G., and Stegman, J.: Optical studies of noctilucent clouds in the extreme ultraviolet, Ann. Geophys., 26, 1109–1119, doi:10.5194/angeo-26-1109-2008, 2008.

Hedin, J., Gumbel, J., Stegman, J., and Witt, G.: Use of O2 airglow for calibrating direct atomic oxygen measurements from sounding rockets, Atmos. Meas. Tech., 2, 801–812, doi:10.5194/amt-2-801-2009, 2009.

Herdrich, G., Auweter-Kurtz, M., Fertig, M., Löhle, S., Pidan, S., and Winter, M.: Present Design of the Flight Instrumentations Pyrex, Phlux and Respect for the Capsule Expert, in: Fifth European Symposium on Aerothermodynamics for Space Vehicles, edited by Danesy, D., vol. 563 of *ESA Special Publication*, pp. 401–408, 2005.

Herron, J. T. and Schiff, H. I.: A Mass Spectrometric Study of Normal Oxygen and Oxygen subjected to Electrical Discharge, Canadian Journal of Chemistry, 36, 1159–1170, doi:10.1139/v58-170, 1958.

Hertz, J. L.: Microfabrication Methods to Improve the Kinetics of the Yttria Stabilized Zirconia-Platinum-Oxygen Electrode, Ph.D. thesis, Massachusetts Institute of Technology, 2006.

Herzberg, G.: Molecular spectra and molecular structure. Vol.1: Spectra of diatomic molecules, 1950.

Kim, J., Samano, E., and Koel, B. E.: Oxygen adsorption and oxidation reactions on Au(211) surfaces: Exposures using O2 at high pressures and ozone (O3) in UHV, Surface Science, 600, 4622–4632, doi:10.1016/j.susc.2006.07.057, 2006.

Laher, R. R. and Gilmore, F. R.: Updated Excitation and Ionization Cross Sections for Electron Impact on Atomic Oxygen, J. Phys. Chem. Ref. Data, 19, 277–305, doi:10.1063/1.555872, 1990.

Lebedev, Y.: Microwave discharges: generation and diagnostics, J. Phys. Conf. Ser., 257, doi:10.1088/1742-6596/257/1/012016, 2010.

Légaré, P., Hilaire, L., Sotto, M., and Maire, G.: Interaction of oxygen with Au surfaces: A LEED, AES and ELS study, Surf. Sci., 91, 175–186, doi:10.1016/0039-6028(80)90078-3, 1980.

Löhle, S., Battaglia, J.-L., Batsale, J.-C., Enouf, O., Dubard, J., and Filtz, R.-R.: Characterization of a Heat Flux Sensor Using Short Pulse Laser Calibration, Rev. Sci. Instrum., 78, doi:10.1063/1.2736388, 2007.

Löhle, S., Fuchs, U., Digel, P., Hermann, T., and Battaglia, J.-L.: Analysing Inverse Heat Conduction Problems by the Analysis of the System Impulse Response, Inverse Probl. Sci. En., 22, 297–308, doi:10.1080/17415977.2013.780170, 2013.

McConkey, J. W., Malone, C. P., Johnson, P. V., Winstead, C., McKoy, V., and Kanik, I.: Electron impact dissociation of oxygen-containing molecules - A critical review, Physics Reports, 466, 1–103, doi:10.1016/j.physrep.2008.05.001, 2008.

Mlynczak, M. G.: Energetics of the Middle Atmosphere: Theory and Observation Requirements, Adv. Space Res., 17, 117–126, doi:10.1016/0273-1177(95)00739-2, 1996.

Munz, C.-D.: Coupled Particle-In-Cell and Direct Simulation Monte Carlo method for simulating reactive plasma flows, C. R. Mécanique, 342, 662–670, doi:10.1016/j.crme.2014.07.005, 2014.

Normand, F., Granier, A., Leprince, P., Marec, J., Shi, M. K., and Clouet, F.: Polymer Treatment in the Flowing Afterglow of an Oxygen Microwave Discharge: Active Species Profile Concentrations and Kinetics of the Functionalization, Plasma Chemistry and Plasma Processing, 15, 173–198, 1995.

Offermann, D. and Drescher, A.: Atomic oxygen densities in the lower thermosphere as derived from in situ 5577-A night airglow and mass spectrometer measurements, Journal of Geophysical Research, 78, 6690–6700, doi:10.1029/JA078i028p06690, 1973.

Offermann, D., Friedrich, V., Ross, P., and von Zahn, U.: Neutral Gas Composition Measurements between 80 and 120 km, Planet. Space Sci., 29, 747–764, doi:10.1016/0032-0633(81)90046-5, 1981.

Oldham, K. B. and Myland, J. C.: Fundamentals of Electrochemical Science, Academic Press, San Diego, 1994.

Osborne, J. J., Harris, I. L., Roberts, G. T., and Chambers, A. R.: Satellite and rocket-borne atomic oxygen sensor techniques, Rev. Sci. Instrum., 72, 4025–4041, doi:10.1063/1.1406928, 2001.

Park, J. H. and Blumenthal, R. N.: Electronic Transport in 8 Mole Percent Y2O3-ZrO2, J. Electrochem. Soc., 136, 2867–2876, doi:10.1149/1.2096302, 1989.

Perov, S. P. and Rakhmanov, A. S.: Atomic Oxygen Concentration Measurements by a Rocket Near the Mesopause, in: Space Research XVII, vol. 17, pp. 261–264, 1977.

Pireaux, J. J., Chtaïb, M., Delrue, J. P., Thiry, P. A., Liehr, M., and Caudano, R.: Electron spectroscopic characterization of oxygen adsorption on gold surfaces: I. Substrate impurity effects on molecular oxygen adsorption in ultra high vacuum, Surf. Sci., 141, 211–220, doi:10.1016/0039-6028(84)90206-1, 1984.

Pulpytel, J., Arefi-Khonsari, F., and Morscheidt, W.: Threshold ionization mass spectrometry study of singlet molecular oxygen in the deposition of SnO2 by PACVD, J. Phys. D, 38, 1390–1395, doi:10.1088/0022-3727/38/9/010, 2005.

Rapp, M., Gumbel, J., and Lübken, F.-J.: Absolute density measurements in the middle atmosphere, Annales Geophysicae, 19, 571–580, doi:10.5194/angeo-19-571-2001, 2001.

Reddy, M. R.: Effect of low earth orbit atomic oxygen on spacecraft materials, J. Mater. Sci., pp. 281–307, doi:10.1007/BF00354389, 1995.

Saliba, N., Parker, D. H., and Koel, B. E.: Adsorption of oxygen on Au(111) by exposure to ozone, Surface Science, 410, 470–482, 1998.

Schmiel, T.: Entwicklung, Weltraumqualifikation und erste Ergebnisse eines Sensorinstruments zur Messung von atomarem Sauerstoff im niedrigen Erdorbit, Ph.D. thesis, Universität Dresden, 2009.

Schrempp, C.: Direct Measurement of Oxygen during a Ballistic Flight on a Sounding Rocket, in: 19th Advanced Measurement and Ground Testing Technology, doi:10.2514/6.1996-2231, 1996.

Schwandt, C. and Weppner, W.: Kinetics of Oxygen Platinum-Stabilized Zirconia and Gold-Stabilized Zirconia Electrodes under Equilibrium Conditions, J. Electrochem. Soc., 144, 3728–3738, doi:10.1149/1.1838083, 1997.

Singh, H., Coburn, J. W., and Graves, D. B.: Appearance potential mass spectrometry: Discrimination of dissociative ionization products, J. Vac. Sci. Technol. A, 18, 299–305, doi:10.1116/1.582183, 2000.

Thomas, R. and Young, R. A.: Measurement of atomic oxygen and related airglows in the lower thermosphere, Journal of Geophysical Research: Oceans, 86, 7389–7393, doi:10.1029/JC086iC08p07389, 1981.

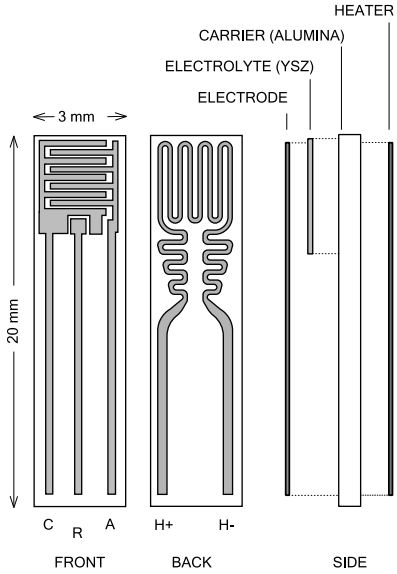

Figure 1. Layout of a FIPEX-sensor. Electrodes are made of platinum, for atomic oxygen sensors the cathode is additionally gold coated.

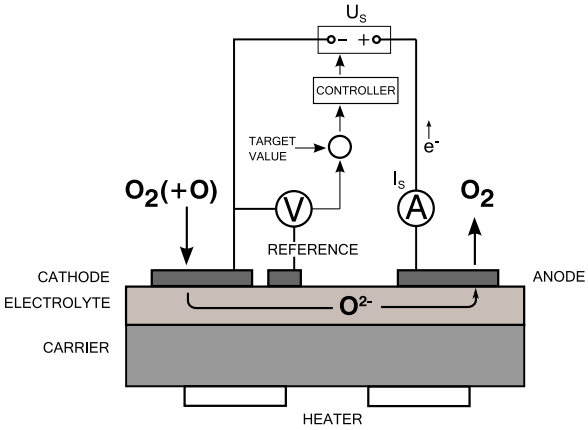

Figure 2. Electrical circuit of a sensor with 3-electrode design and regulation of the reference voltage.

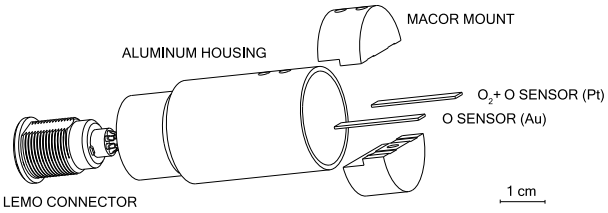

Figure 3. FIPEX head with two sensors (O and $O+O_2$) mounted in a common housing.

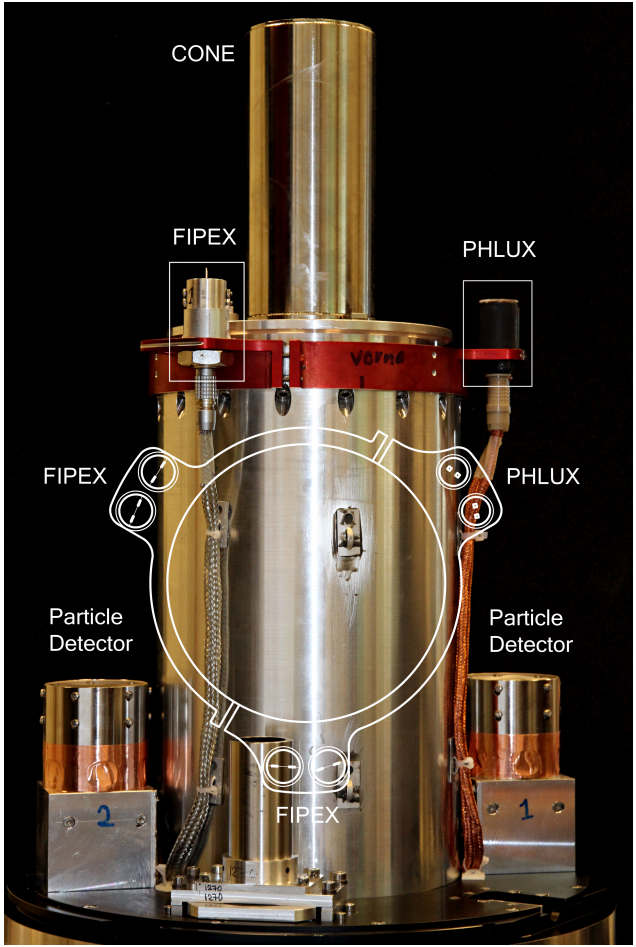
CONE
FIPEX
PHLUX
FIPEX
PHLUX
Particle
Detector
Particle
Detector
FIPEX
2
1

Figure 4. Payload on the fore deck of the rocket with both a FIPEX and PHLUX sensor head visible and a sketch showing their arrangement. Other instruments on the photo are the particle detectors and the CONE ionization gauge, all from IAP. CONE is covered by an evacuated hood.

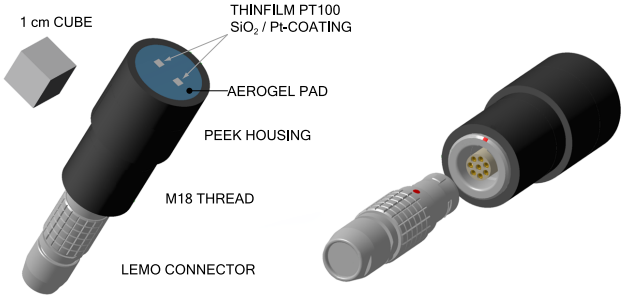

Figure 5. Design of the PHLUX sensor head.

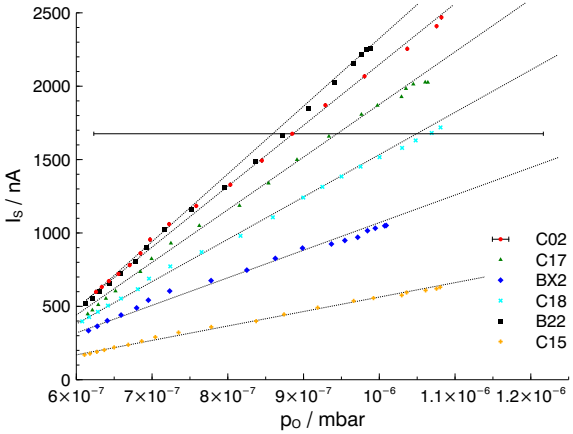

Figure 6. Calibration curves for the atomic oxygen sensors labeled C02..C15 flown on WADIS-1. Sensor currents are plotted over atomic oxygen partial pressure. The error bar represents the uncertainty due to the pressure measurement and shifted electron energy in the QMS ionizer.

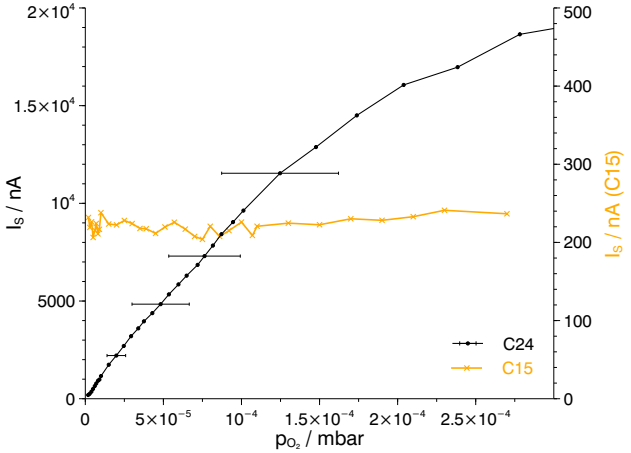

Figure 7. Calibration ~~curve~~ curves for molecular oxygen sensor C24 with platinum electrodes and for atomic oxygen sensor C15 with gold plated cathode. Sensor currents are plotted over the O_2-partial pressure. The error bars indicate the uncertainty due to the pressure measurement.

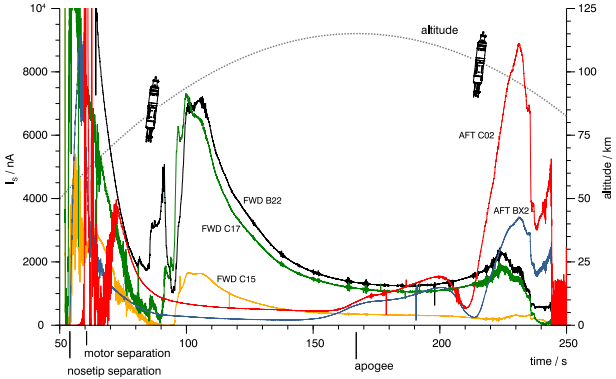

Figure 8. Raw signals of the atomic oxygen sensors versus flight time, together with the altitude and rocket orientation during the experimentation phase.

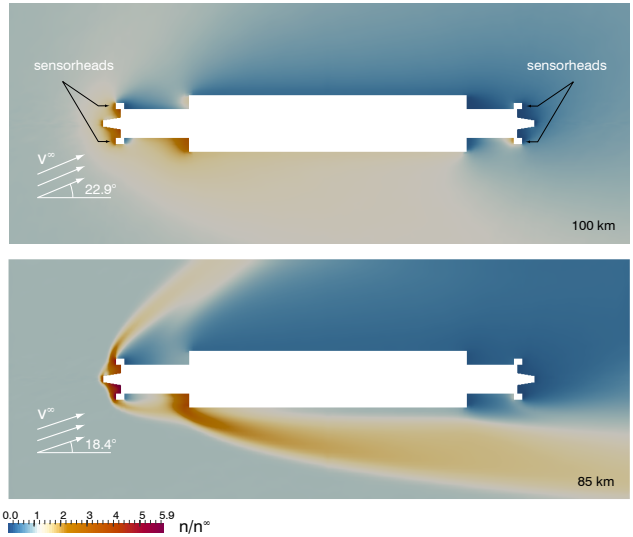

Figure 9. Distribution of the ratio between local and free stream number density during downleg at two different altitudes. Results from 3D DSMC calculations with the PICLas-code.

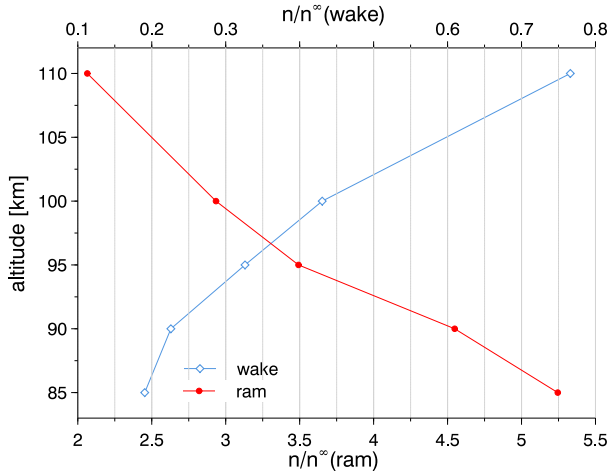

Figure 10. ~~Ratio~~ Ratios between local and free stream total number density at the sensor position as a function of altitude. The ratios are obtained from numerical simulations made at the marked altitudes and are used as aerodynamic correction factors.

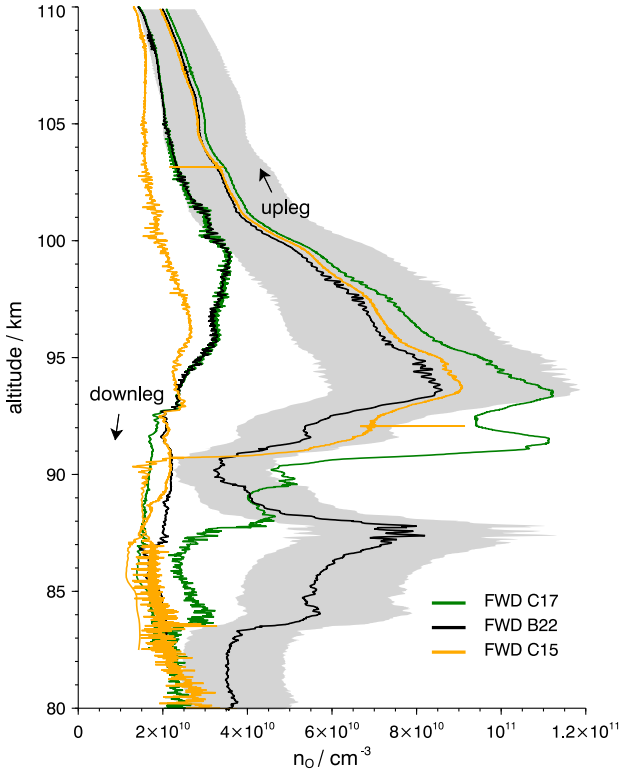

Figure 11. Measurement results for atomic oxygen number density versus altitude for sensors on the fore deck during up- and downleg without aerodynamic correction. The shading shows the uncertainty from the calibration for fore sensor B22.

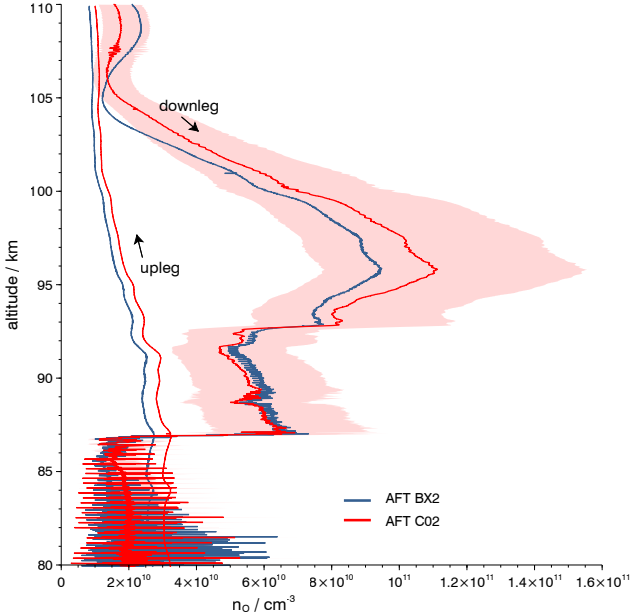

Figure 12. Measurement results for atomic oxygen number density versus altitude for sensors on the aft deck during up- and downleg without aerodynamic correction. The shading shows the uncertainty from the calibration for the aft sensor C02.

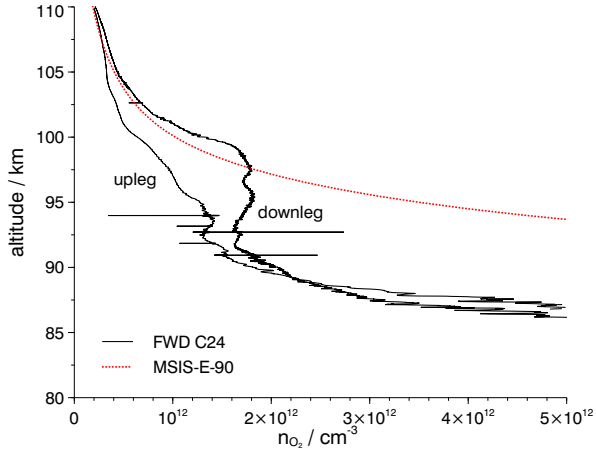

Figure 13. Profile for the O_2 (+O) number density from fore sensor C24 after aerodynamic correction (ram for upleg, wake for downleg) compared to MSIS-E-90.

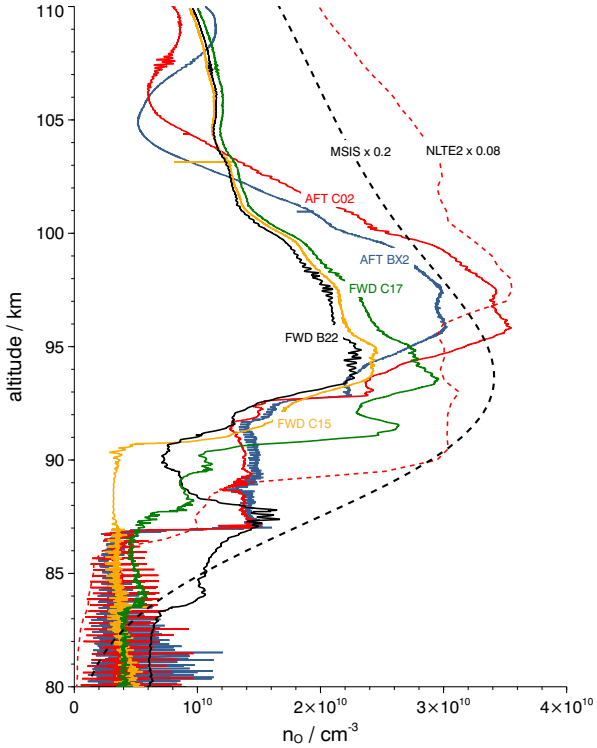

Figure 14. Profiles of O number density for FIPEX sensors on fore and aft deck after aerodynamic ram correction. Downleg profile for aft sensors, upleg part for the fore sensors. ~~The PHLUX profile is scaled by a factor of 1x10^{-3} and is shifted by +16 upwards.~~ Comparison to MSIS model and NLTE-2 measurements.

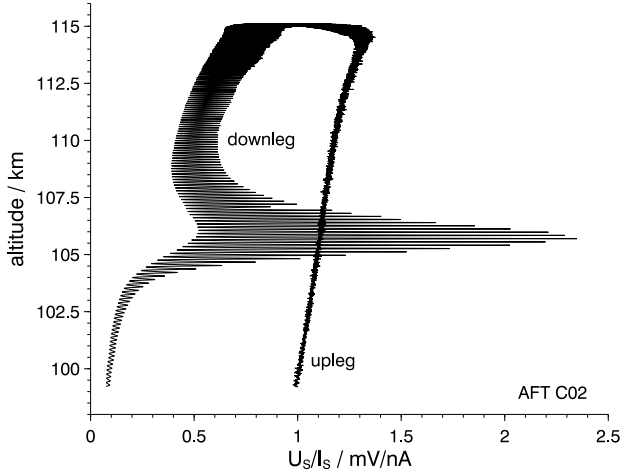

Figure 15. Ratio of voltage to current ~~on~~ for an aft sensor during downleg. Raw values including 2.9 Hz modulation due to rocket spin.

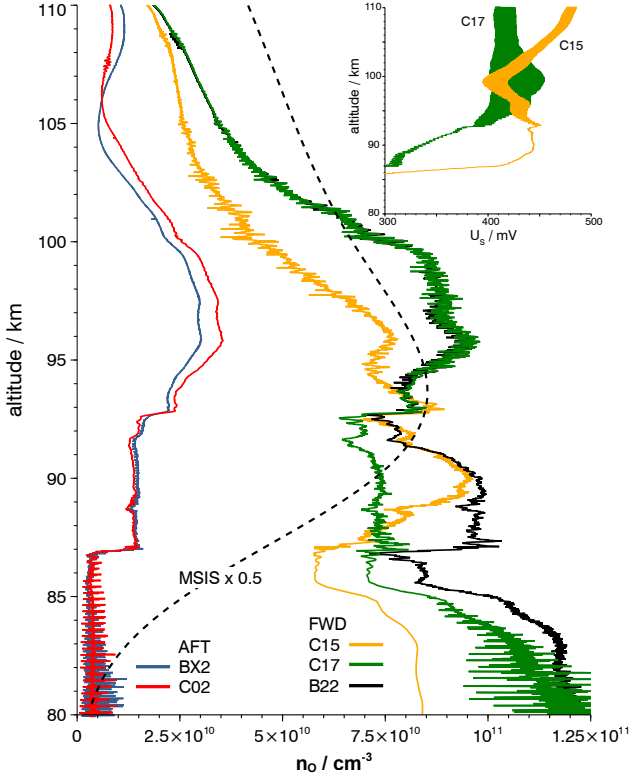

Figure 16. Comparison of O number density profiles from sensors on fore and aft deck during downleg ~~without~~ after aerodynamic correction (ram factors for aft, wake factors for fore). The MSIS profile is scaled by 0.5 and plotted additionally. The inset shows the course of the sensor voltage U_S (including 2.9 Hz-modulation from rocket spin) for two fore-sensors.